Structural properties of $Fe_{60}Mg_{40}$ films grown by coevaporation

1990 J. Phys.: Condens. Matter 2 9907

(http://iopscience.iop.org/0953-8984/2/49/015)

J. Phys.: Condens. Matter **2** (1990) 9907–9917. Printed in the UK

Structural properties of $Fe_{60}Mg_{40}$ films grown by coevaporation

J P Eymery, G Laplanche and A Fnidiki†
Laboratoire de Métallurgie Physique, Unité de Recherche associée au CNRS 131, 40, avenue du Recteur Pineau, F-86022 Poitiers Cédex, France

Received 18 May 1990, in final form 18 September 1990

Abstract. Transmission electron microscopy and Mössbauer effect measurements were made on a coevaporated $Fe_{60}Mg_{40}$ alloy in order to investigate both the initial amorphous state and the amorphous-to-crystalline transition. In the initial state, the nearest-neighbour spacing was determined to be 0.257 nm while the Mössbauer spectroscopy exhibited a doublet, the average quadrupolar separation of which was 0.54 mm s^{-1} at 293 K. A superparamagnetic-like behaviour was also detected at 77 K. The temperature range for the amorphous-to-crystalline transition was found to be 464–482 K. The index μ and activation energy Q in the Johnson–Mehl–Avrami plot were found to be 1 and 310 kJ mol^{-1}, respectively. The transition was clearly a eutectic crystallization of Fe + Mg.

1. Introduction

In thermal equilibrium, binary systems for which the heat ΔH_f of formation is positive generally exhibit a small miscibility in the solid state. For large values of ΔH_f, a miscibility gap over a wide composition range exists even in the liquid state. Therefore, conventional alloying techniques are not applicable for such systems. The recent progress of evaporation techniques for preparing thin films has made it possible to fabricate alloys of completely immiscible element systems for instance by coevaporation or ion beam mixing [1].

In the present work, the same approach has been applied to the Fe–Mg system. In this case, Fe has a BCC structure different to the HCP structure of Mg. The difference in their atomic radii reaches about 30%. These metals are insoluble in each other even in the liquid phase; the value of ΔH_f is close to 23 kJ mol^{-1}. From the literature, it appears that it is possible to form amorphous Fe–Mg alloys by the evaporation technique [2] as well as via superlattices [3–7]. Thus Fe–Mg films are to be regarded as typical artificial materials and for this reason offer an interesting field of research. Here the Mössbauer effect working either in transmission or scattering geometry and transmission electron microscopy (TEM) are combined to study both the initial amorphous state and the

† Present address: Département de Physique, Faculté des Sciences, F-76130 Mont Saint-Aignan, France.

0953-8984/90/499907 + 11 $03.50

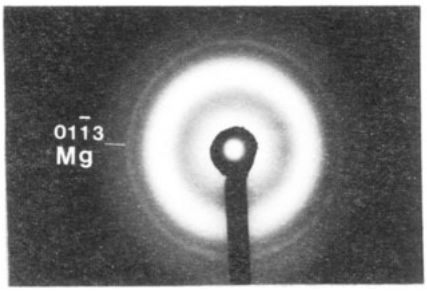

Figure 1. SADP taken at 77 K for as-coevaporated $Fe_{60}Mg_{40}$

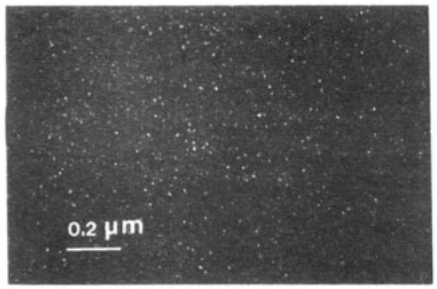

Figure 2. Dark-field image of magnesium zones.

amorphous-to-crystalline (A/C) transition in films of Fe–Mg alloys prepared by co-evaporation.

2. Experimental techniques

The experiment first consisted in preparing coevaporated samples of Fe–Mg alloy, the thickness of which was adjusted according to the requirements of the investigation techniques. The films were deposited using two electron beams installed in a high-vacuum chamber [8]. The starting pressure was 1×10^{-6} Pa and during deposition it was maintained at about $(2–3) \times 10^{-6}$ Pa. The deposition rate of each element, typically 0.2–0.3 nm s^{-1}, and the thickness of the layer were monitored by two quartz oscillators. The following samples were prepared: 100 nm films on NaCl for TEM, 200 nm films on kapton for the conversion electron Mössbauer spectroscopy (CEMS) and 3 μm films also on kapton substrates for the transmission Mössbauer effect (TME). In the latter case, four samples were superposed so that the total thickness analysed was 12 μm.

Microstructural characterization was performed in a JEOL 200 CX transmission electron microscope operating at 200 kV. The composition of the samples was determined by x-ray microanalysis with a Si–Li detector in connection with the microscope. The Mössbauer investigations were conducted using a conventional spectrometer. The electron scattering spectra were taken with a helium flow proportional counter which has recently been described in [9]; a mixture of He–5% CH_4 was allowed to flow through it; the anode was made of two W wires (31 μm in diameter) located apart from the sample surface. However, a single spectrum was taken at 77 K using a channeltron equipped unit working under vacuum. Calibration was achieved with α-iron at room temperature.

3. Results and discussion

3.1. As-coevaporated state

3.1.1. Transmission electron microscopy results. The composition and structure of the thin films were first determined by x-ray microanalysis and TEM. The measured composition of the samples under study was 54.5 at.% Fe and 45.5 at.% Mg. The selected-area diffraction pattern (SADP) taken at 77 K indicates that most of the material is amorphous (figure 1). However, the presence of additional rings indicates the existence

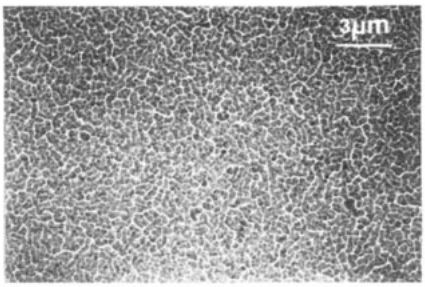

Figure 3. Bright-field image of the initial amorphous state.

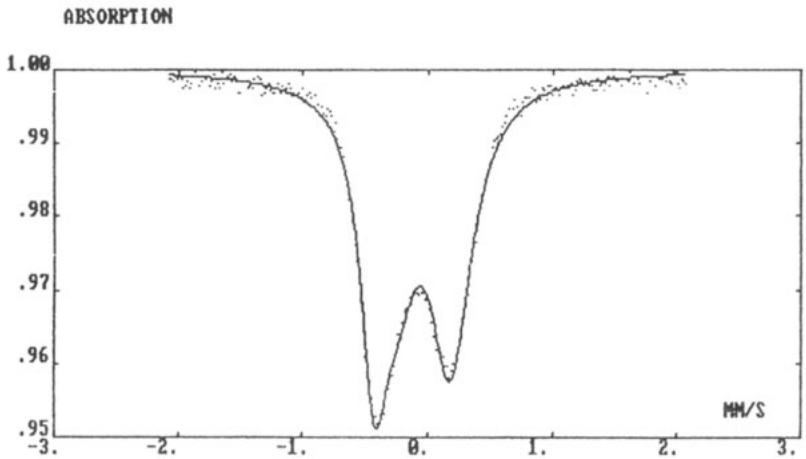

Figure 4. Transmission Mössbauer fitted spectrum at room temperature taken from thick $Fe_{60}Mg_{40}$ films.

of small crystalline zones, the nature of which has been identified to be magnesium. A typical pattern of the magnesium remaining zones is displayed in figure 2 which is a dark-field image taken with a $[01\bar{1}3]$ reflection. A rough estimation of the atomic percentage of free magnesium was about 10% so that the composition of the amorphous alloy would be close to $Fe_{60}Mg_{40}$, a result in agreement with Mössbauer data.

Regarding the initial amorphous state, the structure is depicted in figure 3 which is a bright-field image; it shows a domain morphology close to that described by Phillips [10] and ascribed to accumulated strains. From the SADP, the nearest-neighbour spacing was determined to be 0.257 nm using the Ehrenfest formula. This value is in close agreement with that of other metallic glasses, for instance 0.262 nm in the case of $Ni_{50}Ti_{50}$ amorphized by ion implantation [11].

3.1.2. Transmission Mössbauer effect results. The room-temperature TME spectrum is presented in figure 4 which shows a doublet consisting of two unequal lines. No magnetic splitting has been detected in the $(-8, +8)$ mm s^{-1} velocity range. The average quadrupolar effect and isomer shift were found to be $\Delta = 0.54$ mm s^{-1} and $\delta = 0$ respectively; the total linewidths of the Lorentzian components were 0.36 and 0.45 mm s^{-1} from left to right. The values of the electric interactions are in very good agreement with those

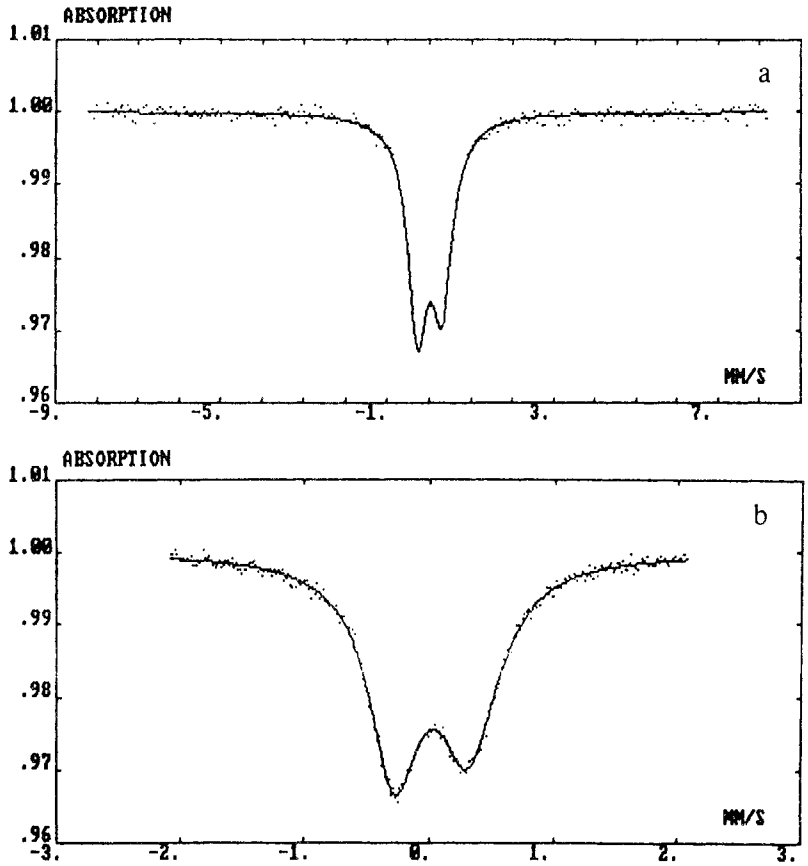

Figure 5. Transmission Mössbauer fitted spectra at 77 K taken from thick $Fe_{60}Mg_{40}$ films in (*a*) the (−8, +8) mm s^{-1} and in (*b*) the (−2, +2) mm s^{-1} velocity range.

determined in [2] and thus strongly support the analysis of the amorphous alloy given in section 3.1.1.

The liquid-nitrogen-temperature TME spectra are shown in figure 5. The spectrum in figure 5(*a*) has been achieved in the (−8, +8) mm s^{-1} velocity range. Although the Curie temperature of the material is $T_C \simeq 200$ K [2], there is no magnetic hyperfine splitting so that the magnetic properties of $Fe_{60}Mg_{40}$ can be understood in analogy with superparamagnetism. The details of the two-line spectrum appear more clearly in figure 5(*b*) which corresponds to the (−2, +2) mm s^{-1} velocity range. The average electric interactions were calculated to be $\Delta = 0.59$ mm s^{-1} and $\delta = 0.13$ mm s^{-1} without correction due to second-order Doppler shift. The linewidths of the components were 0.51 and 0.58 mm s^{-1}.

When comparing the 293 and 77 K spectra, i.e. figures 4 and 5(*b*), it is clear that the second spectrum is slightly broadened with respect to the first spectrum. In order to show this resonance broadening better, an analysis of both spectra using an electric field gradient distribution $P(\Delta)$ was undertaken. The fits were performed by summing eight elementary doublets having the natural linewidth for the spectrum at 293 K and 20 doublets for the spectrum at 77 K. The smoothed distributions $P(\Delta)$ are presented in

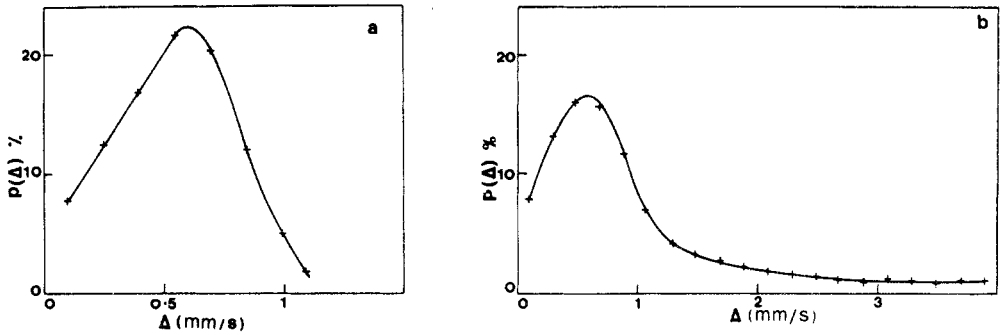

Figure 6. Electric field gradient distributions $P(\Delta)$ corresponding to the Mössbauer spectra in figures 4(*a*) and 5(*b*).

figures 6(*a*) and 6(*b*), respectively. It is satisfactory to note that the shapes of both distributions are nearly the same in the (0, 1.2) mm s^{-1} range. On the other hand, the long tail which appears in figure 6(*b*) at high values of Δ is connected to the resonance broadening observed at 77 K. These results will be discussed in section 3.1.4.

3.1.3. CEMS *results.* Previous spectra concerned samples as thick as 3 μm. Thinner samples (200 nm) were also analysed by the CEMS technique. The 293 K and 77 K spectra are presented in figures 7(*a*) and 7(*b*), respectively. The absence of magnetic splitting is also apparent for thin films. A simple analysis in terms of two lines leads to $\Delta = 0.52$ mm s^{-1} and $\delta = 0$ for the spectrum at 293 K. These results are quite similar to those obtained with thick films. In contrast to the TME spectra, the thin films give nearly the same spectra at both 293 and 77 K. Since $\Delta = 0.54$ mm s^{-1}, there is not much resonance broadening at liquid-nitrogen temperature, which is a result typical of fast relaxation.

3.1.4. Discussion of Mössbauer results. As already mentioned, the magnetic properties of $Fe_{60}Mg_{40}$ could be understood in analogy with superparamagnetism, i.e. the rate of collective fluctuations of the magnetization becomes faster than the nuclear Larmor frequency at 77 K. This suggests that magnetic ordering exists in the alloy at 77 K but the moments with iron atoms are collectively fluctuating. The hypothesis of iron-rich clusters is the most probable, which is not very surprising since Fe and Mg are not usually miscible.

The comparison of the 77 K spectrum of the thick films (3 μm) with that of the thin films (200 nm) indicates a slower relaxation and a faster relaxation, respectively. This suggests that iron-rich clusters would be smaller in thin films than in thick films. However, the determination of the average number of atoms per cluster would require other experiments at lower temperatures as well as the choice of a theoretical model for superparamagnetism. Finally, it should be pointed out that this superparamagnetic-like behaviour has already been observed by Shinjo *et al* [4] for Fe (0.8 nm)/Mg (2.4 nm) multilayers.

3.2. Amorphous-to-crystalline transition

3.2.1. Mössbauer results. The A/C transition has been studied through the variations in spectrum shape as a function of annealing temperature and time. Isochronal and

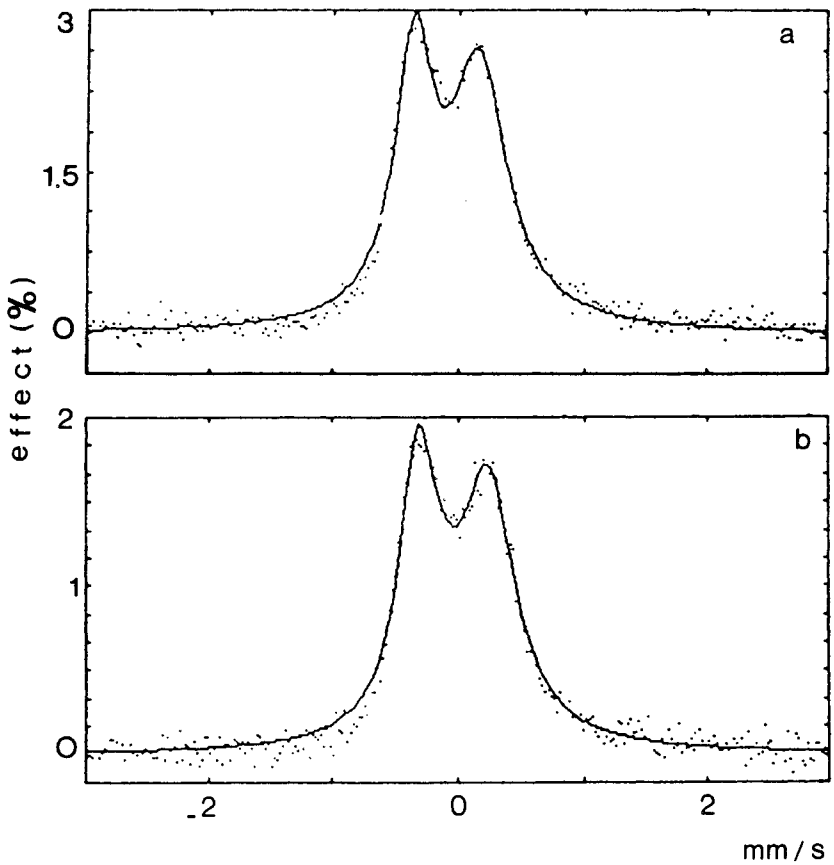

Figure 7. Electron conversion Mössbauer fitted spectra taken from thin $Fe_{60}Mg_{40}$ films at (*a*) 293 K and (*b*) 77 K.

isothermal anneals have been carried out in a small vacuum cell in order to avoid surface contamination. For this purpose a special device was built which was immersed into an oil bath at around 470 K so that the actual temperature of the sample was known with an accuracy of better than 2 K. Both thin (200 nm) and thick (3 μm) films were analysed using CEMS and TME, respectively. A first series of isochronal measurements (1 h) on thick samples was used to obtain a rough estimate of the temperature range of the A/C transition. Then other series were undertaken in order to determine more accurately the variation in crystallized Fe fraction C as a function of time t or temperature T. Special attention was paid to the determination of the Johnson–Mehl–Avrami (JMA) law

$$C = 1 - \exp[-(\alpha t)^{\mu}]$$

where α is the kinetic constant and μ the Avrami exponent which characterizes the crystallization mechanism. The kinetic constant follows an Arrhenius law according to

$$\alpha = \alpha_0 \exp(-Q/RT)$$

where α_0 is a constant, Q the activation energy of the process and R the ideal gas constant.

The temperature range of the AC transition was determined accurately for both kinds of sample. It was found to be very short, namely 464–482 K for thick films and 454–472 K for thin films. The second range is shifted towards lower temperatures by about 10 K with respect to the first one. During the transition, which happens over only 18 K, the Mössbauer spectra consist of both a doublet corresponding to the amorphous component and a sextet corresponding to the crystallized iron containing fraction. In fact, the hyperfine field of the sextet is close to that of α-iron (figure 8 and table 1). It should be noted that the determination of C using the Mössbauer effect does not take into account the crystallized magnesium which can only be detected by TEM.

An isothermal anneal was undertaken at 467 K using thick films in order to determine the Avrami exponent μ. The plot of $\ln[1/(1-C)]$ against t is presented in figure 9 using logarithmic scales. From the slope of the straight line, it is deduced that μ is close to unity (the actual value determined is 0.955). The relatively low value of μ indicates the reaction is probably controlled by external surface growth. Similar results were obtained for thin films.

Isochronal kinetics were also conducted for both kinds of sample in order to calculate the activation energy Q. The A/C transition is well depicted for thin films in both figure 8 and table 1. The annealing temperatures were 467, 476, 481 and 500 K and the annealing time was 1 h exactly. The Mössbauer spectra from a doublet (figure 8(*a*)) towards a sextet (figure 8(*e*)) evolves through intermediary stages where both kinds of component are clearly obvious. The hyperfine interactions together with the values of $1-C$ calculated using a Lorentzian fitting procedure appear in table 1. It should be noted that the hyperfine field of the sextet is somewhat less than that of pure iron; the decrease of about 2% may be attributed to a very small particle size and/or to magnesium substitutions. Similarly, the average quadrupolar effect of the amorphous component slightly decreases with increasing temperature up to 476 K. The values of $1-C$ were used to calculate the activation energy; the plot of $\ln\{\ln[1/(1-C)]\}$ against $1/T$ is presented in figure 10 from which an activation energy of 310 kJ mol^{-1} may be deduced. This value compares quite well with those in the literature for metallic glasses, for instance $Q \simeq 300$ kJ mol^{-1} for Cu–Ti alloys [12]. Finally, it is clear that there is not much difference between thin and thick films.

3.2.2. TEM results. As previously outlined, the thickness of the samples under study was 100 nm. They were heated inside the microscope from room temperature to 550 K. The temperature range of the A/C transition was found to be in agreement with Mössbauer results. A typical pattern of the iron grains is displayed in figure 11 which is a dark-field image taken with a 110 reflection, after a 10 min anneal at 473 K. Crystallization statistics have also been performed at the same temperature from which an average grain size of 20 nm can be calculated. Concerning the end products, both investigation techniques lead to the same conclusion with respect to crystallized α-iron. From the SADP analysis, the following components appear: Mg and MgO; the presence of the latter is easy to understand since the vacuum inside the microscope is not enough to avoid oxidation. From the above results the A/C transition appears to be eutectic.

3.2.3. Discussion. The A/C transition centred at $T_{cr} = 473$ K for thick films then appears to be of eutectic mode as described in detail by Koster [13] for $Al_{50}Ge_{50}$. So it can be inferred that the iron-rich clusters, which have been detected thanks to the Mössbauer spectra taken at 77 K (see sections 3.1.2 and 3.1.4), act as nuclei for iron grain growth. However, no intermediary metastable solid solution has been detected prior to phase

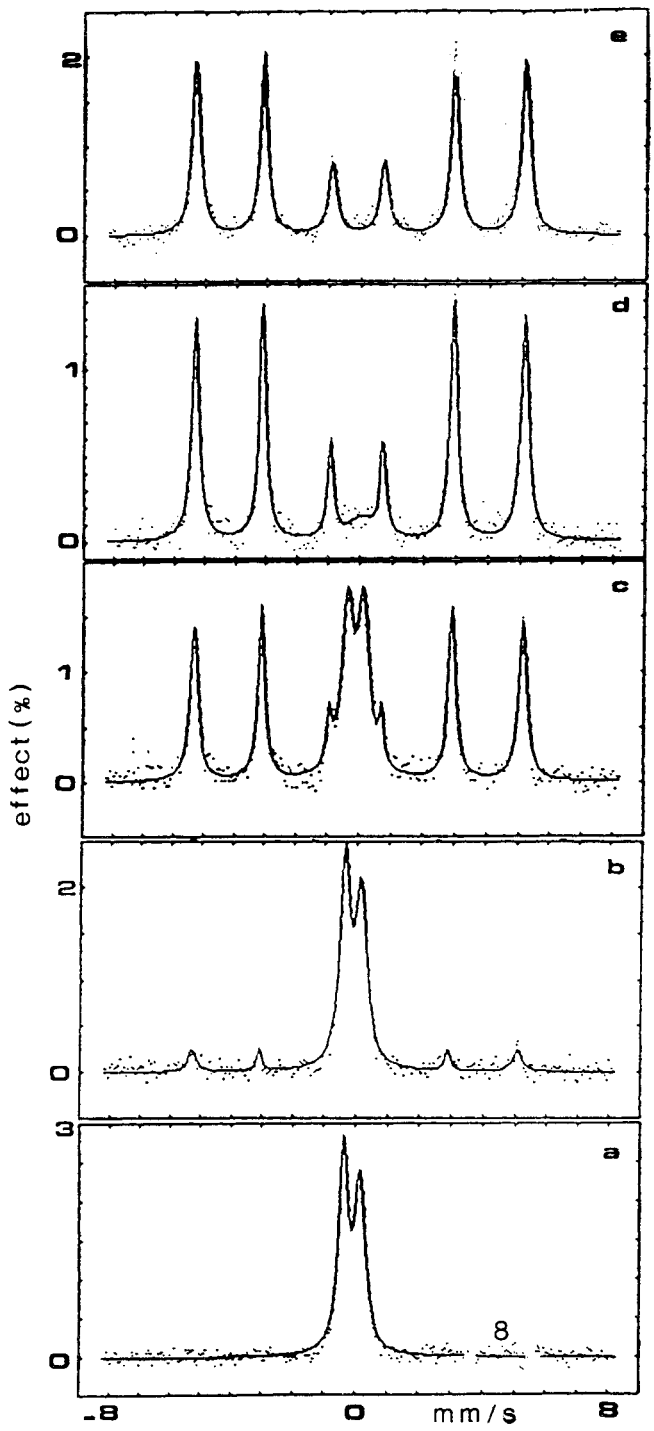

Figure 8. Electron conversion Mössbauer fitted spectra taken at room temperature at various stages of the A/C transition: (*a*) as coevaporated; (*b*)–(*e*) after 1 h anneals at (*b*) 467 K, (*c*) 476 K; (*d*) 481 K and (*e*) 500 K.

Table 1. Fitting results of the Mössbauer electron spectra for thin films during the A/C transition. The errors in the hyperfine field and quadrupole splitting are ±0.1 T and ±0.02 mm s^{-1}, respectively.

Annealing temperature (K)	Hyperfine field of the sextet (T)	Quadrupole splitting of the doublet (mm s^{-1})	Percentage of paramagnetic Fe (%)
293 (as coevaporated)	—	0.54	100
467	32.3	0.50	82
476	32.5	0.49	40.5
481	32.5	—	6.4
500	32.55	—	0

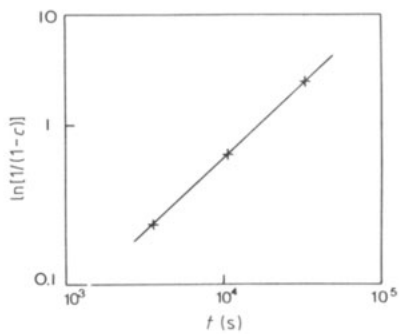

Figure 9. Determination of the index n in the JMA plot where $c(t)$ is the iron-containing crystallized fraction at time t.

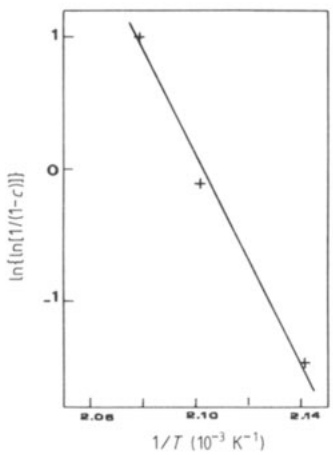

Figure 10. Determination of the activation energy Q in the JMA plot.

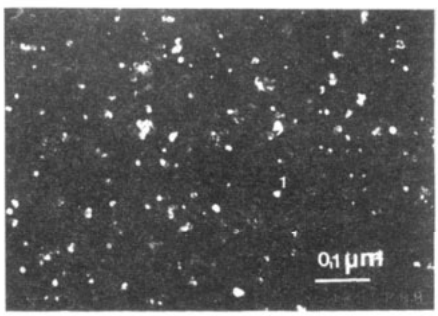

Figure 11. Dark-field image of iron crystallized grains taken after annealing at 470 K for 10 min.

separation as reported by several workers, e.g. Marchal *et al* [14] for the Fe–Au system and Nastasi *et al* [15] for the Cu–W system. The existence of such a metastable solution is supported by considerations of the height of the kinetic barrier. In the present work, it may exist but it is possible that our investigation mode cannot show or has not shown

this. Let us remember that the A/C transition is very sharp; the range is only 18 K when 1 h isochronal anneals are performed.

Although there is no well established correlation between the heat ΔH_f of alloy formation and the crystallization temperature T_{cr}, it is interesting to consider alloys of immiscible elements which exhibit nearly the same values of ΔH_f and T_{cr} as $Fe_{60}Mg_{40}$, for instance $Cu_{45}W_{55}$ [15]. Others which have a lower ΔH_f-value show either a crystallization temperature T_{cr} (when initially amorphous) or a decomposition temperature T_d (when initially crystalline) which is higher. The Fe–Ag alloys, for which $\Delta H_f = 10$ kJ mol^{-1} and $T_d = 570$ K [16], are an example of the latter. In the case of compounds possessing a negative heat of formation, Buschow [17] showed that a relation actually existed between T_{cr} and the vacancy heat ΔH_v of formation in amorphous materials:

$$T_{cr} = 7.5\,\Delta H_v$$

where ΔH_v is expressed in kilojoules per mole. The basic physical idea was that the instability of amorphous alloys was directly connected to the heat of formation and motion of point defects. Nevertheless Nastasi *et al* [15] have pointed out that compounds possessing a positive heat of formation deviated more from this law when ΔH_v was high. When the above Buschow relation is applied to $Fe_{60}Mg_{40}$, one obtains $T_{cr} \simeq 560$ K, which is slightly higher than the experimental value, the deviation being about 90 K. However, the experimental results which were used to establish the Buschow relation exhibit some dispersion so that, as a first approximation, one can still note that this relation is roughly obeyed in the case of $Fe_{60}Mg_{40}$.

4. Conclusion

Amorphous $Fe_{60}Mg_{40}$ films were grown by electron gun coevaporation in an initial vacuum of 1×10^{-6} Pa. Using TEM and the Mössbauer effect, the structure of the as-evaporated state as well as the A/C transition were investigated for so-called thin (100–200 nm) films and thick (3 μm) films.

From SADPs, the nearest-neighbour spacing was determined to be 0.257 nm in the amorphous state. The Mössbauer effect gave a two-line spectrum at 293 K for both kinds of sample. Although the Curie temperature was 200 K, the spectra taken at 77 K remained doublets instead of sextets. This behaviour was understood by analogy with superparamagnetism, thus leading to the hypothesis of iron-rich clusters.

The temperature of the A/C transition was determined for both thin and thick films; it was found to be 464–482 K for thick films and 454–472 K for thin films. The second range was slightly shifted towards lower temperatures with respect to the first range. The exponent μ in the JMA law was about unity while the activation energy Q was 310 kJ mol^{-1}. We infer a eutectic crystallization of Fe + Mg but the kinetic model of Buschow is only roughly obeyed.

References

[1] Peiner E and Kopitzki K 1988 *Nucl. Instrum. Methods* B **34** 173
[2] Van der Kraan A M and Buschow K H J 1982 *Phys. Rev.* B **25** 3311
[3] Shinjo T, Kawaguchi K, Yamamoto R, Hosoito N and Takada T 1984 *Solid State Commun.* **52** 257
[4] Shinjo T, Kawaguchi K, Yamamoto R, Hosoito N and Takada T 1985 *Thin Solid Films* **125** 273

[5] Shinjo T 1986 *Hyperfine Interact.* **27** 193
[6] Kawaguchi K, Yamamoto R, Hosoito N, Shinjo T and Takada T 1986 *J. Phys. Soc. Japan* **55** 2375
[7] Shinjo T, Hosoito N, Kawaguchi K, Nakayama N, Takada T and Endoh Y 1986 *J. Magn. Magn. Mater.* **54–7** 737
[8] Jaulin M, Laplanche G, Delafond J and Pimbert-Michaux S 1989 *Surf. Coat. Technol.* **37** 225
[9] Bodin D and Eymery J P 1986 *Nucl. Instrum. Methods* B **16** 424
[10] Phillips J C 1981 *J. Physique Coll. Suppl* 10 **42** C4 197
[11] Bodin D, Moine P and Eymery J P 1987 *Nucl. Instrum. Methods* B **23** 337
[12] Hwang Ch, Kang S and Cho K 1985 *Scr. Metall.* **19** 1403
[13] Köster U 1984 *Amorphous Metals and Non Equilibrium Processing* (Les Ulis: Les Editions de Physique) pp 175–86
[14] Marchal G, Mangin P and Janot C 1975 *Phil. Mag.* **32** 1007
[15] Nastasi M, Saris F W, Hung L S and Mayer J W 1985 *J. Appl. Phys.* **58** 3052
[16] Kataoka N, Sumiyama K and Nakamura Y 1989 *Acta Metall.* **37** 1135
[17] Buschow K H J 1982 *Solid State Commun.* **43** 171